Supporting Information

Chemical Fabrication and Synergistic Mechanism of N-doped Carbon Modified with FeP as Catalysts for Flexible Rechargeable Zn-Air Batteries

Xianli Wu, [a,#] Ting Zhou, [a,#] Guosheng Han, [a] Shuling Liu, [a] Mengmeng Cao, [a] Shuqi Li, [b] Jiawen Wang, [a] Yanyan Liu,[a,b,c*] Jianchun Jiang, [c] Yongfeng Wang, [d] Baojun Li [a,e]

[a] College of Chemistry, Zhengzhou University, 100 Science Road, Zhengzhou 450001, P R China

[b] College of Science, Henan Agricultural University, 63 Nongye Road, Zhengzhou 450002, P R China

[c] Institute of Chemical Industry of Forest Products, CAF, National Engineering Lab for Biomass Chemical Utilization, Nanjing 210042, P R China

[d] Center for Carbon-based Electronics and Key Laboratory for the Physics and Chemistry of Nanodevices, Department of Electronics, Peking University, Beijing 100871, P.R. China

[e] Department of Chemistry, Tsinghua University, Beijing 100084, P. R. China

[#] These Authors contribute equally to this work

* Corresponding author. E-mail: lyylhs180208@163.com (Y.Y. Liu)

† Electronic Supplementary Information (ESI) available: Some characterization results. See DOI: 10.1039/x0xx00000x

1. Experimental section

1.1 Characterization

On an X-ray diffractometer (Bruker, D8 Advance, Cu K = 1.5418 Å), powder X-ray diffraction (PXRD) patterns of as-prepared materials were obtained. The Raman spectrum was obtained using a Renishaw RM-2000 and an Air-ion laser (= 514 nm). Scanning electron microscopy (SEM, ZEISS Sigma 500) and transmission electron microscopy (TEM, FEI Tecnai G^2 F20 S-TWIN electron microscope, operating at 200 kV) were used to examine the morphologies of as-prepared materials. On a Thermo Scientific ESCALAB 250 instrument, X-ray photoelectron spectroscopy (XPS) was performed. The XPSPEAK41 program was used to fit the XPS data. Shirley served as the backdrop tape for all high-resolution XPS spectra. The ASAP 2460 analyzer (USA) was used to carry out the N_2 adsorption-desorption studies at 77.3 K. The surface area was determined using the Brunauer-Emmett-Teller (BET) method, and the nonlocalized density functional theory was used to examine the catalyst's pore size distribution (NLDFT).

1.2 Electrochemical measurements

All electrochemical measurements of ORR were performed on a CHI 760E. Electrochemical Analyzer with rotating disk electrode (RDE) or rotating ring disk electrode (RRDE) as working electrode, Pt wire as the counter electrode, and Ag/AgCl as a reference electrode. The working electrodes were bought from Pine. The electrolyte of reference electrode is a saturated KCl solution. In this work, all electrode potentials were referenced to the reversible hydrogen electrode (RHE) based on the following

calculation equations:

$$E_{vs\,RHE} = E_{vs\,Ag/AgCl} + 0.059\mathrm{pH} + 0.197 \qquad (1)$$

The electrode working area of the rotating disk electrode (RDE) is 0.196 cm^2 and the rotating ring-disk electrode (RRDE) is 0.217 cm^2. The RRDE consists of a glassy carbon disk (GC) surrounded by a Pt ring, while there is only a GC in the center of the RDE. The catalyst ink was prepared by ultrasonic dispersion of 4 mg catalyst in a hybrid solution including 500 μL ethanol and 50 μL Nafion.15 μL ink was coated onto working electrode. CV measurements were carried out in O_2/N_2-saturated 0.1 M KOH solution in the voltage range of 0–1.2 V for all the samples with a scan rate of 50 mV s^{-1}. LSV measurements were carried out in O_2-saturated 0.1 M KOH solution at different rotating rates from 400 to 2025 rpm with a scan rate of 5 mV s^{-1}. Tafel slopes were obtained from the Tafel equation:

$$E = a + b\log|J_k| \qquad (2)$$

E is the applied potential of LSV tests, and *a* is a constant, *b* is the Tafel slope and J_k is the kinetic current density.

Moreover, the Kinetic properties of ORR were also carried out with RRDE in an O_2-saturated 0.1 M KOH solution with a scan rate of 5 mV s^{-1}. The yields of peroxide species and the electron transfer number can be calculated from the LSV of RRDE measurement at 1600 rpm via the following equation:

$$n = 4\frac{I_D}{I_D + I_R/N} \qquad (3)$$

$$H_2O_2(\%) = 200\frac{I_R/N}{I_D + (I_R/N)} \qquad (4)$$

The I_D is the disk current and I_R is the ring current. The N represents the current collection efficiency equaled to 0.41 of the RRDE in our experimental system.

The accelerated durability test (ADT) was performed by CV in 0.1 M O_2-saturated KOH solution for 5000 cycles with a scan rate of 50 mV s^{-1}. Methanol resistance was measured by adding methanol to 100 mL 0.1 M KOH under 800 rpm at the 400th second. The concentration of CH_3OH in the electrolyte was 1 M. The chronoamperometry test was performed on FeP@NPW at 0.8 V for 22 h in O_2-saturated 0.1 M KOH solution on the RDE at 800 rpm. For the OER, the polarization curves were also recorded in voltage range of 1.1-1.9 V and the scan rate is 5 mV s^{-1}. To avoid the peeling of the catalyst caused by evolved O_2 adhesion, a rotation speed of 1600 rpm was offered during the OER. The electrochemical active surface area (ECSA) was calculated by comparing the double-layer capacitance (C_{dl}) of the electrocatalysts, with higher C_{dl} exhibiting greater ECSA. C_{dl} was measured by cyclic voltammetry (CV) at different scan speeds (5, 10, 15, 20, 25, and 30 mV s^{-1}) inside the non-Faradaic potential window. The C_{dl} value was calculated as the slope of a straight line from the plot of current density (half the sum of absolute values of current density at 1.10 V vs RHE) vs scan rate. The results of electrochemical impedance spectroscopy (EIS) were acquired over a frequency range of 0.01 to 100 kHz.

1.3 Zinc-air battery test

For aqueous Zinc-air batteries, FeP@NPW powder catalyst was loaded on carbon fiber and used as the air electrode. FeP@NPW ink was prepared by taking 4 mg FeP@NPW powder, 320 μL ethanol, 80 μL deionized water and 16 μL Nafion. The ink was drip-

coated on 2 cm×2 cm carbon paper with a pipetting gun, and then dried at 60℃ for 3h to obtain the catalytic layer of air electrode. In the 20% Pt/C+RuO_2 ink, 20% Pt/C and RuO_2 are both 2 mg, and the other conditions are the same as FeP@NPW. 6 M KOH and 0.2 M $Zn(OAc)_2$ were used as the electrolyte. The electrolyte was able to circulate between the positive and negative electrodes under the drive of a small motor. A Celgard 2340 microfiber filter was utilized as a separator. A polished high-purity Zinc plate was chosen as the negative electrode. The flexible Zinc-air battery was assembled by using Zinc foil (3 cm * 1 cm * 0.03 cm) as an anode, integrated FeP@NPW as air electrode, and nickel foam as current collector. The gel electrolyte was placed between Zinc anode and air electrode.

2. Supplementary Figures and Tables

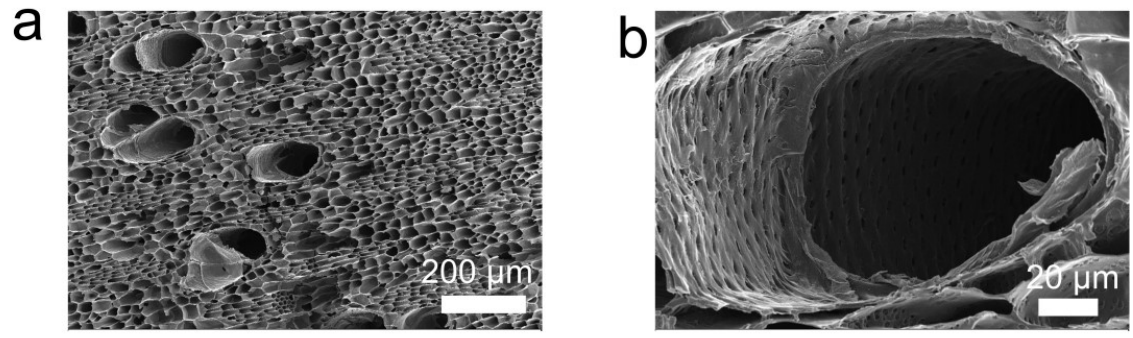

Fig.S1. SEM images of PW.

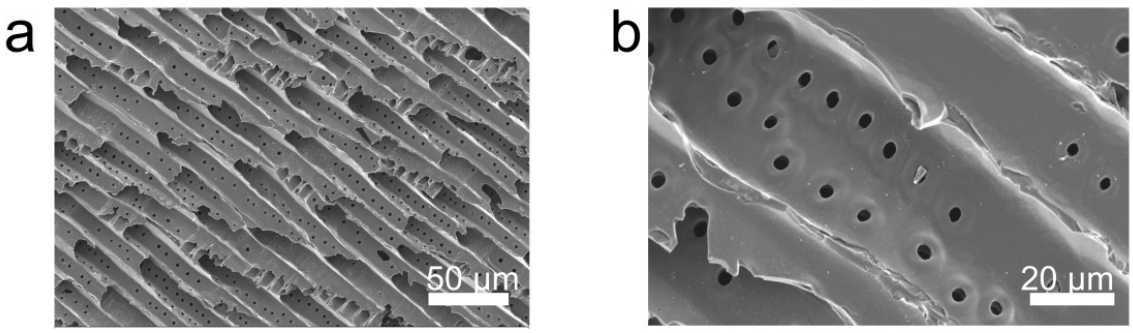

Fig. S2. SEM images of NPW

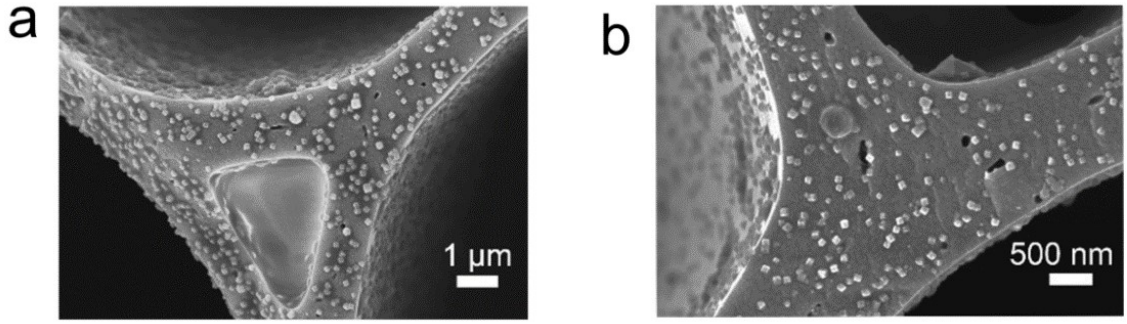

Fig. S3. SEM images of PB@NPW(a); SEM images of FeP@NPW(b).

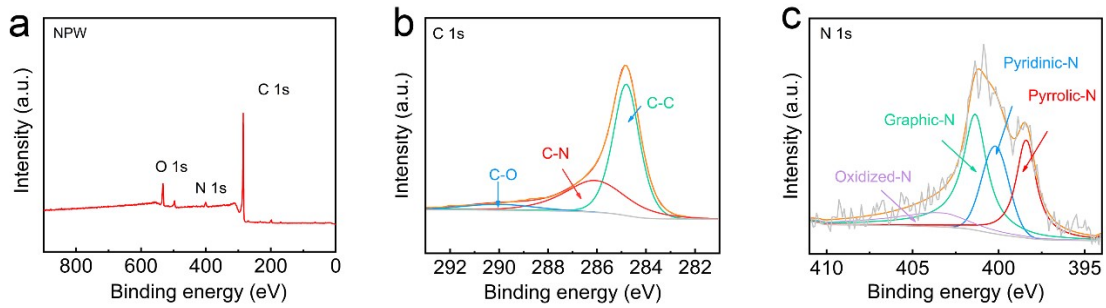

Figure S4. (a) the XPS survey spectrum of NPW. High-resolution XPS spectra and corresponding residual plots of (b) C 1s and (c) N 1s

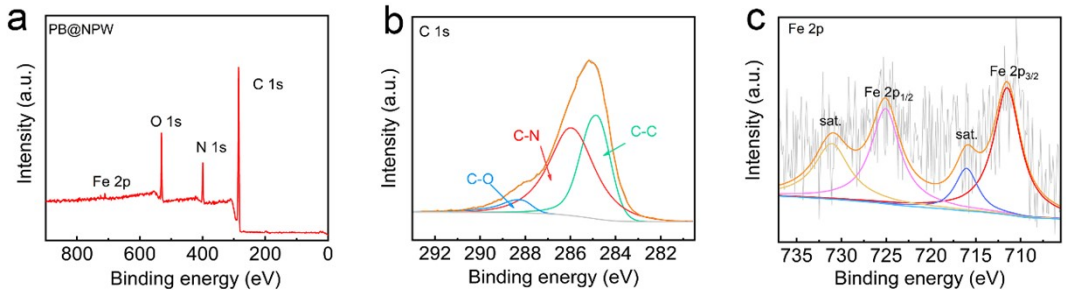

Figure S5. (a) the XPS survey spectrum of PB@NPW. High-resolution XPS spectra and corresponding residual plots of (b) C 1s and (c) Fe 2p

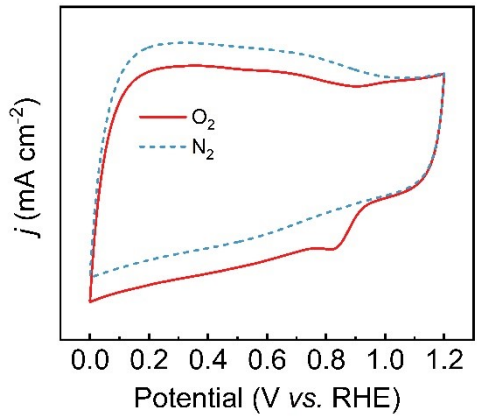

Fig. S6. CV curves of FeP@NPW in O_2/N_2-saturated 0.1 M KOH.

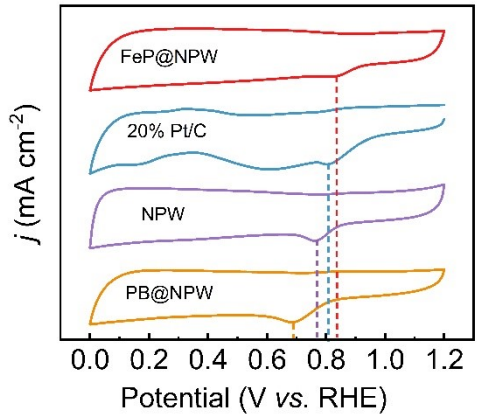

Fig. S7. CV curves of FeP@NPW, PB@NPW, NPW, and Pt/C in O_2-saturated 0.1 M KOH.

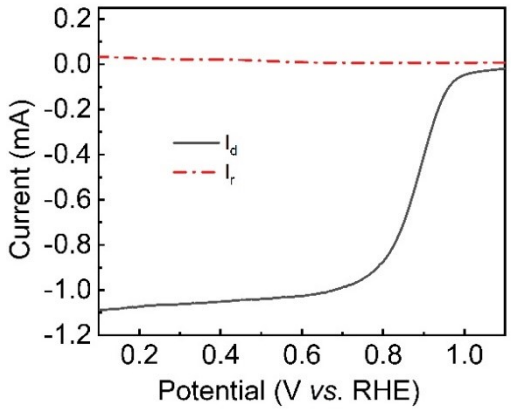

Fig. S8. Disk and ring current obtained by LSV on a RRDE for FeP@NPW.

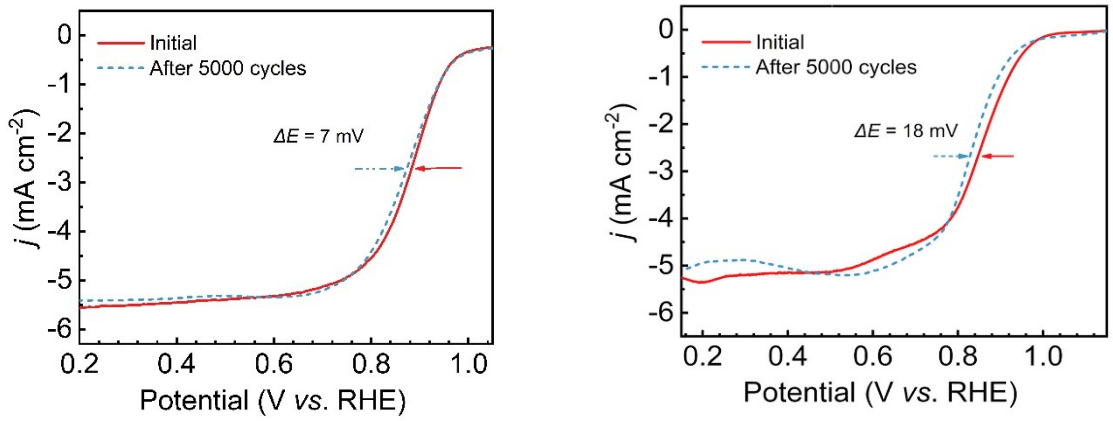

Fig. S9. The LSV curves of FeP@NPW (a) 20% Pt/C (b) and before and after accelerated durability test.

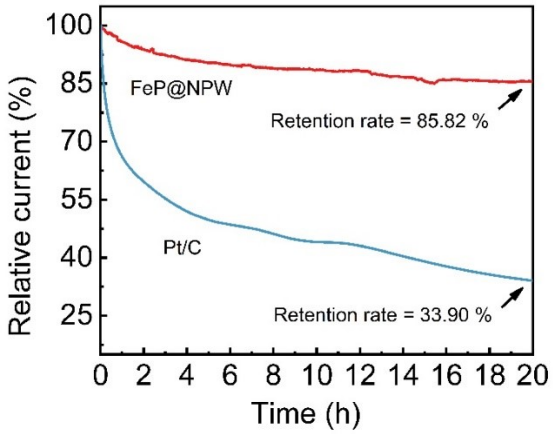

Fig. S10. Chronoamperometric response of FeP@NPW and 20% Pt/C.

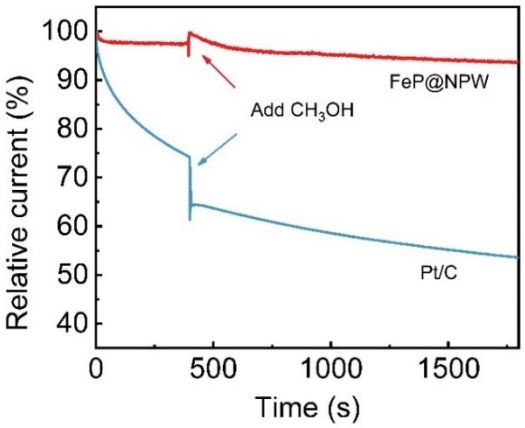

Fig. S11. Methanol tolerant tests of FeP@NPW and 20% Pt/C.

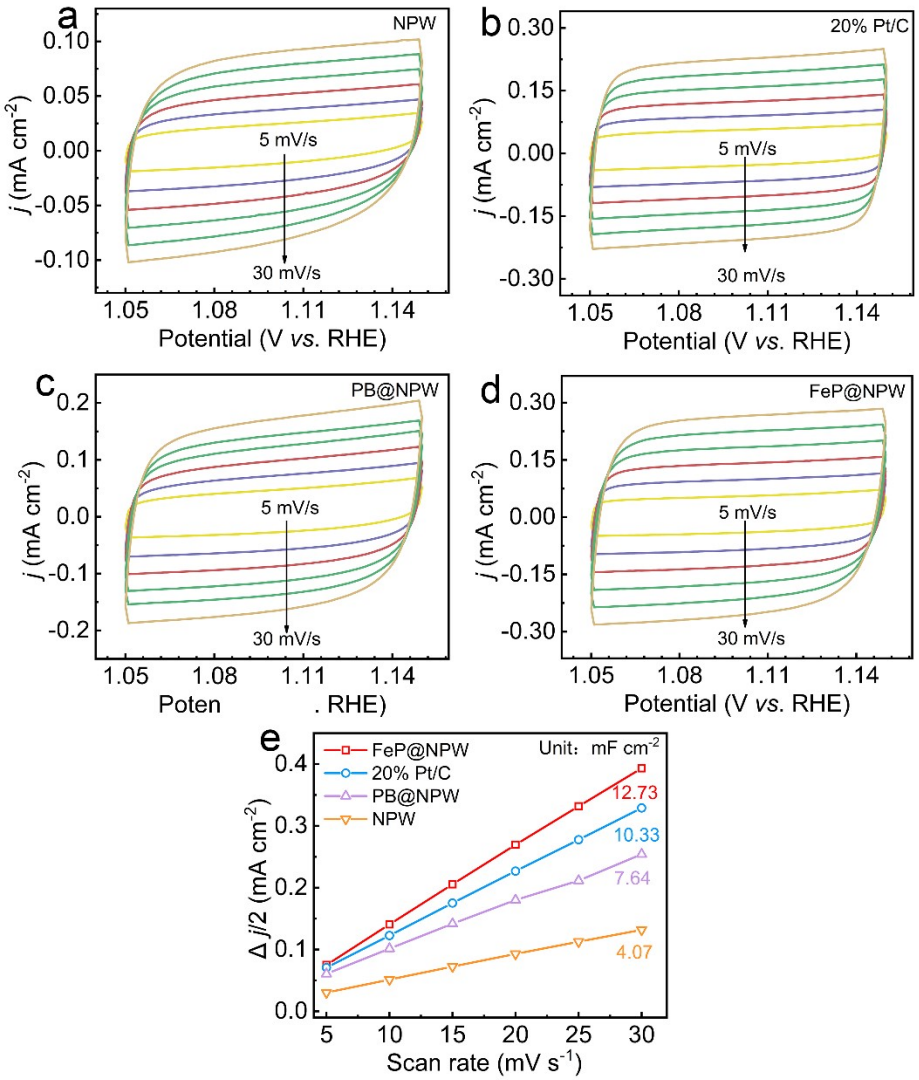

Fig. S12. CV curves of (a) NPW, (b) Pt/C, (c) PB@NPW, (d) FeP@NPW at various scan rates from 5 to 30 mV s^{-1}, (e) The summarized double layer capacitance (Cdl) of all sample, (f) Nyquist plots of FeP@NPW, PB@NPW, NPW, and Pt/C.

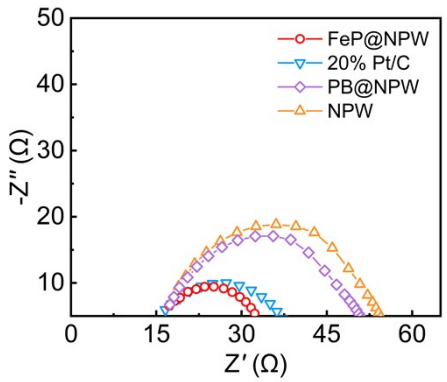

Fig. S13. Nyquist plots of FeP@NPW, PB@NPW, NPW, and Pt/C.

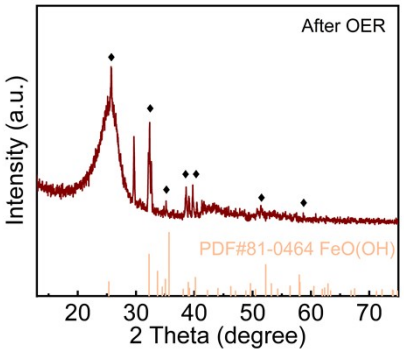

Fig. S14. XRD patterns of FeP@NPW before and after OER.

Table S1. Element analysis result of FeP@NPW determined by XPS.

Catalyst	C (at.%)	N (at.%)	Fe (at.%)	P (at.%)	O (at.%)
Co-BTC-bipy-700	74.3	3.3	2.3	3.0	17.1

Table S2. Bifunctional performance comparison of FeP@NPW the electrocatalyst with non-precious metal catalysts in alkaline solution.

Catalyst	$E_{1/2}$	$E_{j=10}$	ΔE	Reference
FeP@NPW	0.88	1.53	0.65	**This work**
FeCo/Se-CNT	0.90	1.65	0.75	[1]
FePc||CNTs||NiCo/C	0.90	1.58	0.68	[2]
Co-N-PCN	0.82	1.61	0.79	[3]
Fe-NSDC	0.84	1.64	0.80	[4]
CoSAs@CNT	0.86	1.64	0.78	[5]
Fe-NC SAC	0.88	1.68	0.80	[6]
CoN4/NG	0.87	1.61	0.74	[7]

Co_9S_8/CNT	0.82	1.59	0.78	[8]
FeMn-DSAC	0.92	1.63	0.71	[9]
FeCo-ACM	0.90	1.60	0.70	[10]
Mn SAC	0.91	1.58	0.67	[11]
Ni_2P_5@NCNT	0.77	1.59	0.82	[12]
LO-NF-NCNs	0.77	1.71	0.94	[13]
Co-BTC-bipy-700	0.79	1.63	0.84	[14]

References

1. Y. Sha, Y. Peng, K. Huang, L. Li, Z. Liu, *Adv. Energy Mater.,* 2022, **12**, 2200906.

2. H. Zhang, M. Zhao, H. Liu, S. Shi, Z. Wang, B. Zhang, L. Song, J. Shang, Y. Yang, C. Ma, L. Zheng, Y. Han, W. Huang, *Nano Lett*., 2021, **21**, 2255–2 264.

3. Y. Tang, R. Liu, S. Liu, B. Zheng, Y. Lu, R. Fu, D. Wu, M. Zhang, M. Rong, *Carbon*, 2019, **141**, 704–711.

4. J. Zhang, M. Zhang, Y. Zeng, J. Chen, L. Qiu, H. Zhou, C. Sun, Y. Yu, C. Zhu, Z. Zhu, *Small*, 2019, **15**, 1900307.

5. S. Dilpazir, H. He, Z. Li, M. Wang, P. Lu, R. Liu, Z. Xie, D. Gao, G. Zhang, *ACS Appl. Energy Mater.,* 2018, **1**, 3283–3291.

6. C. Du, Y. Gao, J. Wang, W. Chen, *J. Mater. Chem. A*, 2020, **8**, 9981–9990.

7. L. Yang, L. Shi, D. Wang, Y. Lv, D. Cao, *Nano Energy,* 2018, **50**, 691–698.

8. H. Li, Z. Guo, X. Wang, *J. Mater. Chem. A*, 2017, **5**, 21353–21361.

9. T. Cui, Y.-P. Wang, T. Ye, J. Wu, Z. Chen, J. Li, Y. Lei, D. Wang, Y. Li, *Angew. Chem. Int. Ed.,* 2022, **61**, e202115219.

10. C. Chen, D. Cheng, S. Liu, Z. Wang, M. Hu, K. Zhou, *Energy Stor. Mater.,* 2020, **24**, 402–411.

11. H. Shang, W. Sun, R. Sui, J. Pei, L. Zheng, J. Dong, Z. Jiang, D. Zhou, Z. Zhuang, W. Chen, J. Zhang, D. Wang, Y. Li, *Nano Lett.,* 2020, **20**, 5443–5450.

12. J. Lv, S.C. Abbas, Y. Huang, Q. Liu, M. Wu, Y. Wang, L. Dai, *Nano Energy*, 2018, **43**, 130–137.

13. Z. Wang, F. Zhang, C. Jin, Y. Luo, J. Sui, H. Gong, R. Yang, *Carbon*, 2017, **115**, 261–270.

14. X. Zhang, J. Luo, H.-F. Lin, P. Tang, J.R. Morante, J. Arbiol, K. Wan, B. W. Mao, L. M. Liu, J. Fransaer, *Energy Stor. Mater.,* 2019, **17**, 46–61.